Unicluster Dissociation of Large Alkali Iodide Cluster Ions†

Joseph E. Campana* and Brian N. Green‡

Contribution from the Naval Research Laboratory, Chemistry Division, Washington, DC 20375, and VG Analytical Ltd., Floats Road, Wythenshawe, Manchester, UK M23 9LE.
Received August 1, 1983

Abstract: The gas-phase dissociation of a series of high-mass alkali halide cluster ions, produced by particle bombardment on alkali halide solids, has been studied by state-of-the-art mass spectrometric techniques. The previously reported anomalous regions or distinct deviations in the cluster ion abundance distributions originate from the unicluster decay of certain structurally unstable cluster ion species. The unicluster and bimolecular dissociation pathways have been determined for the cluster ion species about one anomalous region, and the mode of decay is dependent on the chemical identity of the cluster ion species. A voltage biasable collision cell has allowed the observation of some consecutive dissociation reactions in a conventional mass spectrometer, and this particular observation has led to a novel concept for the study of consecutive reactions in a mass spectrometer. This method, based on tandem collision cells in a single field-free region, is discussed. Finally, a secondary cluster ion emission mechanism for the alkali halide system is presented, which is consistent with these new findings on the origin of the anomalous regions.

Secondary ion mass spectrometry (SIMS) and fast atom bombardment mass spectrometry (FABMS) have allowed the production, mass analysis, and detection of a series of ultra-high-mass alkali halide (MX) cluster ions of the type $[M(MX)_n]^+$ and $[X(MX)_n]^-$. Cesium iodide (CsI) secondary cluster ion abundance distributions were obtained to $n = 70$ or m/z 18 320[1,2] on a double-focusing SIMS instrument.[3] All of the alkali halides have shown strong anomalous regions in their secondary cluster ion spectra, defined by significant deviations at certain n values from the general pseudexponential envelope of the secondary cluster ion distribution. For example, the $n = 13$ cluster ion abundance is enhanced relative to the $n = 12$ cluster ion abundance while the $n = 14$ and $n = 15$ cluster ion abundances dramatically drop below the envelope. Several anomalous regions have been observed; the next occurs at $n = 22$, 23, and 24. The ion abundance enhancement at the first n value in each anomalous region has been attributed to very stable cubic-like structures. For example, the $n = 13$ species ($[M(MX)_{13}]^+$) containing 27 atomic species corresponds to a $3 \times 3 \times 3$ (three atomic species per edge) cubic structure for the simple cubic salts or a $3 \times 3 \times 3$ rhombohedral structure for the body-centered cubic salts. Likewise, the $[M(MX)_{22}]^+$ species corresponds to the $3 \times 3 \times 5$ structure. Other anomalous regions, some of which are ionic radii and crystal structure dependent, are described elsewhere.[1,2,4,5]

Ultrahigh-mass FABMS spectra[6] of $[Cs(CsI)_n]^+$ ($n = 99$, m/z 25 854), $[I(CsI)_n]^-$ ($n = 87$, m/z 22 730), $[Na(NaI)_n]^+$ ($n = 54$, m/z 8117), and $[I(NaI)_n]^-$ ($n = 59$, m/z 8971) were obtained on a reverse-geometry spectrometer.[7,8] Additionally, a simple bond-breaking model has been developed,[9] which qualitatively describes the various pseudexponential shapes of the envelopes from the ultrahigh secondary cluster ion abundance distributions of these different salts.[10]

An intriguing feature of the mass spectra obtained on the latter double-focusing spectrometer is the decreased prominence of the so-called anomalous regions. The ion abundances within the anomalous regions were shown to vary as a function of the cluster ion flight time (100–200 μs) to the detector.[7] We concluded from these observations that the anomalous ion abundance regions were a result of unimolecular dissociations or, more appropriately, unicluster dissociations of the cluster ions.[11]

Independent SIMS studies on CsI were performed on a time-of-flight (TOF) mass spectrometer[12,13] where the mass spectra recorded corresponded to the ion abundance distributions at very short times (<200 ns) after the cluster ions were emitted. (Fragment ions from dissociations occurring after acceleration but during the flight to the detector in a TOF spectrometer appear at the same m/z value as the parent ion.) The resultant TOF secondary cluster ion distribution is similar to those we previously reported with the double-focusing SIMS instrument; however, anomalous regions are not observed in the TOF data. Cluster ion dissociation products in the TOF studies were identified by use of a retarding potential grid placed prior to the detector to discriminate against those ions having undergone unicluster dissociation, since they have less than the full kinetic energy. These TOF data independently confirm that the origin of the anomalous regions, especially the dramatic negative deviations, is a result of unicluster decay.

This report focuses on positive and negative ion unicluster and collision-induced dissociation of CsI and NaI cluster ions about the first anomalous region ($n = 13$–15). Single-focusing mass spectrometric data of unicluster dissociation of the various clusters are presented, and the dissociation pathways intrinsic to each species are discussed. Mass-analyzed ion kinetic energy spectrometry (MIKES) data of unicluster and bimolecular (cluster/molecule) dissociations are presented and discussed. When a voltage potential was applied to the collision cell of the MIKES spectrometer, consecutive reactions occurring in the second field-free region of the spectrometer were identified. An instrumental scheme is proposed, based on this novel observation, to

† This paper was presented in part at the 31st Annual Conference on Mass Spectrometry and Allied Topics, May 8-13, 1983, Boston, MA.

* Address correspondence to this author at the Naval Research Laboratory.

‡ VG Analytical Ltd.

(1) J. E. Campana, T. M. Barlak, R. J. Colton, J. J. DeCorpo, J. R. Wyatt, and B. I. Dunlap, *Phys. Rev. Lett.*, **47**, 1046–1049 (1981).
(2) T. M. Barlak, J. R. Wyatt, R. J. Colton, J. J. DeCorpo, and J. E. Campana, *J. Am. Chem. Soc.*, **104**, 1212–1215 (1982).
(3) Mattauch–Herzog geometry: R. J. Colton, J. E. Campana, T. M. Barlak, J. J. DeCorpo, and J. R. Wyatt, *Rev. Sci. Instrum.*, **51**, 1685–1689 (1980).
(4) T. M. Barlak, J. E. Campana, R. J. Colton, J. J. DeCorpo, and J. R. Wyatt, *J. Phys. Chem.*, **85**, 3840–3844 (1981).
(5) T. M. Barlak, J. E. Campana, J. R. Wyatt, and R. J. Colton, *J. Phys. Chem.*, **87**, 3441–3445 (1983).
(6) Although a liquid sample matrix was not used in these studies as is conventional in FABMS, we refer to these data as FABMS. The differences in the SIMS and FABMS spectra reported here are due to other instrumental differences (vide infra) and not the identity of the primary particle, i.e., ions versus neutrals.
(7) J. E. Campana, R. J. Colton, J. R. Wyatt, B. N. Green, and R. H. Bateman, *Appl. Spectros.*, in press.
(8) B. I. Dunlap, J. E. Campana, B. N. Green, and R. H. Bateman, *J. Vac. Sci. Technol. A*, **1**, 432–436 (1983).
(9) B. I. Dunlap, *Surf. Sci.*, **121**, 260–274 (1982).
(10) J. E. Campana and B. I. Dunlap, *Int. J. Mass Spectrum. Ion Proc.*, in press.
(11) T. M. Barlak, J. E. Campana, J. R. Wyatt, B. I. Dunlap, and R. J. Colton, *Int. J. Mass Spectrom. Ion Phys.*, **46**, 523–526 (1983).
(12) W. Ens, R. Beavis, and K. G. Standing, *Phys. Rev. Lett.*, **50**, 27–30 (1983).
(13) K. G. Standing, R. Beavis, W. Ens, and B. Schueler, *Int. J. Mass Spectrom. Ion Phys.*, **53**, 125–134 (1983).

study consecutive reactions in the second field-free region of a conventional reverse-geometry (MIKES) spectrometer. A simulation of this scheme with use of tandem collision cells is presented for consecutive dissociations of $C_5H_{10}O$. Finally, in light of these findings on unicluster decay, a discussion is given on the possible origin of the large cluster ions observed in our studies.

Experimental

The mass and MIKES spectra reported here were obtained on a VG Analytical Ltd ZAB-HF mass spectrometer. This instrument is a double-focusing instrument of the reverse geometry (magnetic sector precedes electrostatic sector). This reverse-geometry instrument permits operation of the mass spectrometer in the single-focusing mode (low resolution) or the double-focusing mode (high resolution) where an ion-detection system can be operated at the focal points of the magnetic sector or electrostatic sector. Each of the two detectors consists of a stainless-steel conversion dynode and a EMI 17-stage venetian blind type copper-beryllium electron multiplier placed opposite each other and perpendicular to the ion beam. The ion beam (positive or negative) is postaccelerated by 5 keV into the conversion dynode, and the secondary electrons emitted from the conversion dynode are accelerated into the first stage of the electron multiplier (operated at 2 kV, 4×10^3 gain). This dynode/multiplier arrangement allows transmission of the ion beam into the second sector for double-focusing and MIKES operation when the voltages are absent from the first detector arrangement. Additionally, in the MIKES mode an ion of interest is mass selected in the single-focusing mode, and fragment ions resulting from unimolecular and bimolecular dissociations that occur between the sectors (second field-free region) are energy analyzed by the electrostatic analyzer. The second field-free region collision cell allows the application of a voltage for the purpose of differentiating (in the energy spectrum) those dissociations occurring within the collision cell from those dissociations occurring external to the collision cell.[14] This instrument used a high-field magnet (2.3 T) allowing an ultimate mass of approximately m/z 3250 to be analyzed at an 8-kV acceleration potential. (The mass range is inversely proportional to the acceleration potential.) The NaI data were obtained at 8-keV acceleration potentials whereas the CsI data were obtained at 6-keV acceleration potentials. Reference 14 describes the general features and design of the basic ZAB-type instrument.

The instrument was fit with a fast atom bombardment ion source and saddle-field gun (Ion Tech Ltd, Teddington, Middlesex, UK TW11 0LT[15]) that was operated at 8 kV and approximately 3.0 mA with xenon as the discharge gas. A primary ion deflector was placed at the exit of the saddle-field gun to assure that only fast neutrals would impinge on the sample. Other details of this arrangement are discussed in ref 10.

The reagent grade alkali halides (CsI and NaI) were dissolved in water, the sample holder (NiCr) dipped in the aqueous solution, and the water evaporated in vacuo. The salts were not placed in a liquid matrix (e.g., glycerol) as in the usual FABMS experiments.[16] Nevertheless, these experiments will still be referred to as FABMS (neutral bombardment) throughout—FABMS differs from SIMS (ion bombardment) only by the charge state of the bombarding species.

The ion signal was detected with conventional analog electronics, and the speectra were recorded with an oscillographic recorder from which the ion abundances were measured directly. The general features of the envelope from the FABMS spectra were similar to those we obtained on our double-focusing SIMS instrument.[1-5]

Results and Discussion

(A) Unicluster Reactions. Metastable peaks due to the dissociation of large positive and negative cluster ions were observed and reported in our early cluster studies.[3,4] However, the instrumental limitation of a short second field-free region[17] limited the abundance of the metastable peaks, and an instrumental artifact was responsible for metastable peaks so grossly skewed that the peak centroids could not be determined. These factors limited our initial studies on metastable alkali halide species to simple processes.[4]

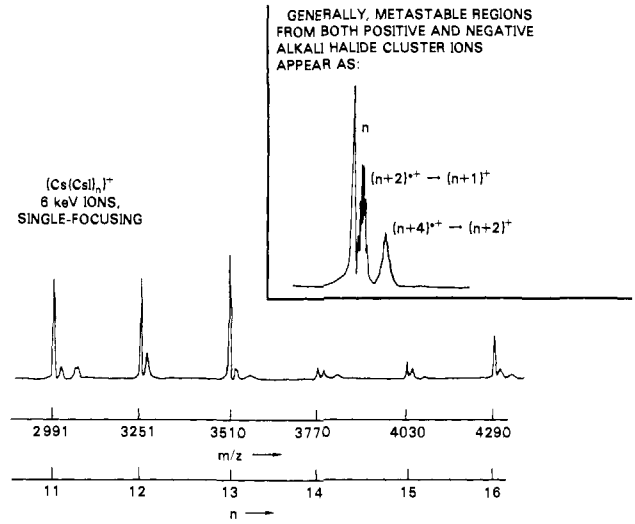

Figure 1. Conventional single-focusing secondary ion mass spectrum of CsI showing the trend in the metastable peaks generally observed for alkali halides. The region from $n = 11$ to 16 about the first anomalous region ($n = 13$–15) is shown. The general dissociations yielding the metastable peaks are shown in the inset.

Table I. Some Positive and Negative Metastable Alkali Iodide Cluster Ion Abundances[a]

metastable decomp[b]	$[Cs(CsI)_n]^+$	$[I(CsI)_n]^-$	$[Na(NaI)_n]^+$	$[I(NaI)_n]^-$
11 → 10	11	7	5	3
11 → 9	25	15	20	25
12 → 11	21	15	6	5
12 → 10	10	5	25	18
13 → 12	18	12	6	6
13 → 11	6	4	19	24
14 → 13	460	160	35	4
14 → 12	51	11	34	40
15 → 14	31	20	20	6
15 → 13	180	57	285	25
16 → 15	40	20	7	7
16 → 14	9	4	35	22
17 → 16	64	37	13	9
17 → 15	15	7	57	36

[a] The ion abundances are in percent, relative to the precursor ion abundance. These were measured by peak area. [b] The dissociation is given in terms of the cluster ion n value.

The mass spectra obtained in the single-focusing mode[18] of the reverse-geometry spectrometer[14] show strong conventional metastable peaks. Metastable peaks for the dissociation $m_1^+ \rightarrow m_2^+ + m_3$ will appear at an apparent mass-to-charge ratio (m/z); $(m/z)^* = (m_2/z)^2/(m_1/z)$. Figure 1 shows a single-focusing CsI cluster ion mass spectrum from $n = 11$ to 16, which is representative of the other subject cluster ion mass spectra. The pairs of broad metastable stable peaks at the $(m/z)^*$ slightly above the m/z of the n-valued cluster ions correspond to two unicluster dissociations. These dissociations are

$$[M(MX)_{n+2}]^{+*} \rightarrow [M(MX)_{n+1}]^+ + MX$$

and

$$[M(MX)_{n+4}]^{+*} \rightarrow [M(MX)_{n+2}]^+ + 2MX$$

where n corresponds to the preceeding n-valued cluster ion as shown in the inset of Figure 1.

The ion abundance of the metastable peak (fragment ion abundance) relative to the precursor ion abundance gives an

(14) R. P. Morgan, J. H. Beynon, R. H. Bateman, and B. N. Green, *Int. J. Mass Spectrom. Ion Phys.*, **28**, 171–191 (1979).
(15) J. Franks, *Int. J. Mass Spectrom. Ion Phys.*, **46**, 343–346 (1983).
(16) M. Barber, R. S. Bordoli, G. J. Elliott, E. D. Sedgwick, and A. N. Tyler, *Anal. Chem.*, **54**, 645A–657A (1982).
(17) Metastable peaks appear in the mass spectra obtained on a Mattauch–Herzog geometry (double-focusing) instrument[3,4] when dissociations occur in the region between the electrostatic analyzer (first sector) and the magnetic sector (second field-free region).
(18) Metastable peaks in a single-focusing mass spectrometer arise from dissociations occurring between the object slit and the entrance to the magnetic sector (first field-free region).
(19) T. P. Martin, *J. Chem. Phys.*, **72**, 3506–3510 (1980).

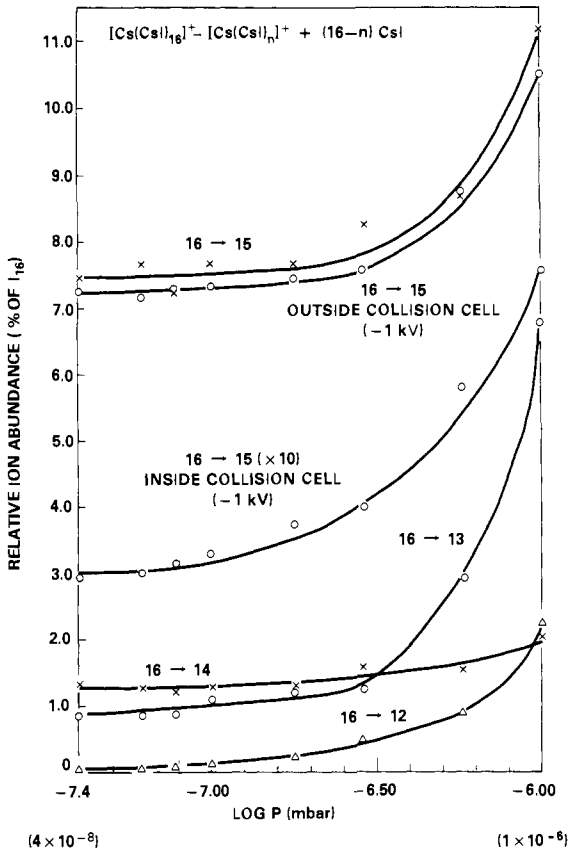

Figure 2. The relative fragment ion abundances of the CsI n = 16 species obtained by MIKES is shown as a function of collision-gas pressure. The ultimate vacuum of the system is 4×10^{-8} mbar. The relative abundance of the n = 15 collision-product ion, derived from collisions between the sectors taking place inside and outside the collision cell, is shown. These latter values were determined by placing a −1-kV potential on the collision cell. The other relative ion abundances are for the total of all dissociation processes occurring between the sectors.

indication of the cluster ion stability and the energetically favored dissociation pathways. Table I gives these data. The positive and negative ion CsI data show that unicluster dissociation occurs by the dominant loss of one molecule from the cluster ion. The exceptions are the dissociation of the n = 15 species, which preferentially loses two molecules to yield the stable rhombohedral n = 13 cluster ion, and the dissociation of the n = 11 species, which preferentially loses two molecules to give the stable stacked hexagonal structures[1,2,4,5,19] at n = 9 (vide infra). On the other hand, the NaI positive cluster ions dissociate by loss of two molecules except for the n = 14 species, which preferentially dissociates by the loss of one molecule to yield the stable cubic n = 13 cluster ion. These studies do not indicate whether the loss of two molecules is a consecutive or concerted loss.

The NaI negative cluster ion spectrum does not show strongly anomalous ion abundance regions.[7,10] This may indicate that the NaI negative cluster ions at n = 14 and 15 have less tendancy to decay to more compact (stable) clusters or that their rates of unicluster decay vary less dramatically with n than the corresponding positive ion rates. Table I shows that the NaI negative cluster ions, n = 11 through 17, all decay by preferential loss of two molecules. At this time we cannot explain the absence of anomalous regions in the negative ion NaI data.

The unicluster data reported here are time dependent as evidenced by the double-focusing[7,11] and TOF studies.[12,13] We have measured this time dependency over a limited mass and time range,[7] and it should be emphasized that these results are valid only in the time domain of the double-focusing experiments reported here (ca. 80–200 μs).

(B) Collisional Reactions. Although the metastable dissociation data presented in the previous section are quite informative, additional fragmentation pathways and the nature of stable cluster

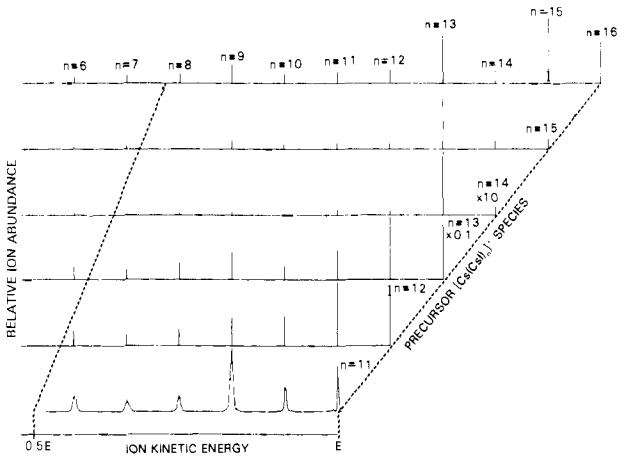

Figure 3. The relative fragment ion abundances from the CID-MIKES spectra of the n = 11–16 CsI precursor cluster ions. The n = 13 precursor ion abundance is attenuated by a factor of 10, and the n = 14 precursor ion abundance is magnified by a factor of 10. Stable structures exist at n = 6, 9, 12, 15 (stacked hexagonal rings) and at n = 13 (3 × 3 × 3 rhombohedron).

fragment ions can be determined by collision-induced dissociations (CID).[20] There is some question as to whether the observed unicluster dissociations are indeed metastable or whether they are, in fact, bimolecular (cluster/molecule) dissociations resulting from extremely high collision cross sections of highly excited cluster ions. Figure 2 shows a plot of the relative ion abundance of various fragment ions from the CsI n = 16 species vs. the pressure external to the collision cell in the second field-free region (helium collision gas). This illustrates that in the ultimate vacuum (4×10^{-8} mbar) of the spectrometer, unicluster processes predominate; it is not until a collision-gas pressure of about twice the ultimate vacuum is reached (1×10^{-7} mbar) that an increase in fragmentation occurs (collision-induced dissociations). The collision cross sections of these cluster ions are higher than those of organic ions that we have studied. For example, the n = 16 ion abundance is attenuated almost 90% at a pressure of 1×10^{-6} mbar whereas the ion abundance of organic species such as $[C_6H_5]^+$ is attenuated about 50% at the same pressure.

Figure 3 shows the CID-MIKES spectra of the CsI n = 11 – 16 cluster ions (precursor ions). The n = 6, 9, 12, and 15 CsI cluster ion abundances appear enhanced (stable) in these CID-MIKES spectra as well as the conventional mass spectra.[1,2,5] The enhanced ion abundance of these species is attributed to stable, cationized, stacked hexagonal ring structures,[1,2,4,5] which also have been shown to be stable structures in theoretical studies.[19] The n = 13 species (shown attenuated by 10 in Figure 3) is stable while the unstable n = 14 species (shown magnified by 10) predominantly dissociates to give the highly stable n = 13 species. The relatively stable n = 16 species dissociates to the stable stacked hexagonal ring structure at n = 15 as well as the rhombohedral n = 13 species. This alternative stable n = 15 structure apparently does not exist in significant abundance for the NaI clusters formed by the sputter emission mechanism; consequently, the NaI n = 15 species readily dissociates. The relative rates of dissociation of the n = 14 and 15 species can be inferred by comparing the ratio of the fragment cluster ion abundances for their dissociation pathways shown in Table I.

The decreased stability of the n = 14 and 15 species relative to the stable cubic-like structure at n = 13 can be rationalized by consideration of cluster surface energy.[1,2] The two cluster species immediately following the stable one would be expected to have high surface energy regions as a result of incomplete cubic faces. However, when a third molecule is added (for example, n = 16), the relative surface energy of the cluster ion will decrease because a face of the three atomic species edge structure is $^2/_3$

(20) R. G. Cooks, Ed. "Collision Spectroscopy", Plenum Press, New York, 1978.

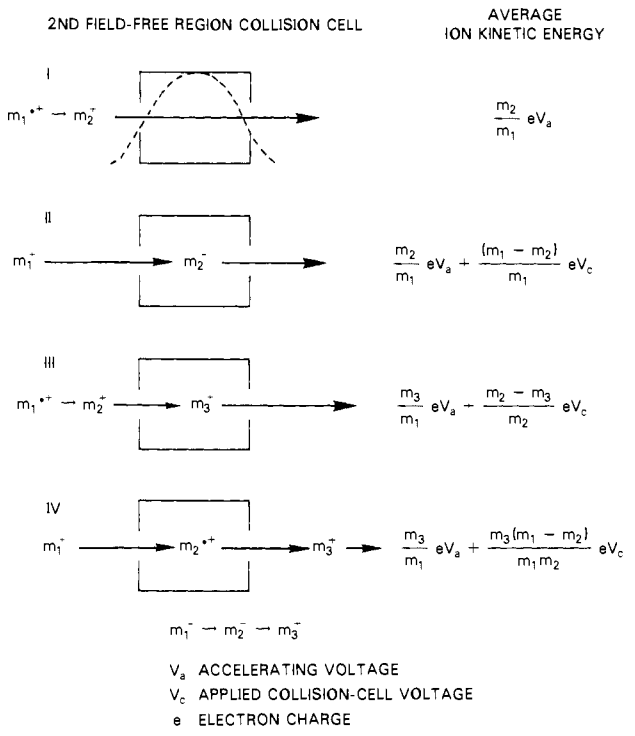

Figure 4. The resultant average ion kinetic energy is given for the (I) single-step dissociation occurring outside the collision cell, (II) the CID reaction occurring within the cell with a voltage V_c applied, (III) the consecutive reaction where the first step occurs prior to the cell and the second step occurs within the cell, and (IV) the consecutive reaction where the first step occurs inside the cell followed by the second step after the cell. A pressure profile through the collision-cell region is depicted (I), demonstrating that the collision gas is not bounded by the collision cell.

filled forming a step on the cube. This consideration can also be used to explain the other higher anomalous regions[10] and supports our belief that cubic-like rather than other isomers typically dominate at each value of n.

(C) **Consecutive Reactions.** The high-collision cross sections of these cluster ions allow sucessive collisional activation of the precursor and the resultant daughter ions at collision-gas pressures low enough that fragment ion loss due to scattering is negligible. Therefore, novel consecutive dissociation reactions are observed in the second field-free region of the MIKES spectrometer when the voltage-bisable collision cell is used. Figure 4 shows the four reactions that can be observed with the instrumental arrangement. The average kinetic energy of the product ions, m_2^+ from a single dissociation (Figure 4, I and II) and m_3^+ from consecutive reactions (Figure 4, III and IV), is shown.

Also illustrated in Figure 4I is the fact that the collision gas pressure distribution across the second field-free region does not go to the ultimate vacuum (4×10^{-8} mbar) at the cell boundaries. Therefore, bimolecular dissociations also will occur in the high-pressure region just outside the collision cell, and these bimolecular processes might be interpreted as unimolecular processes when the cell voltage bias feature is used to distinguish (in the energy spectrum) those dissociations occurring internal and external to the cell. This is illustrated further in Figure 2 where the dissociation of the CsI $n = 16$ species to the $n = 15$ species is resolved into a bimolecular and unimolecular component with the cell bias voltage. This shows that the number of dissociations occurring just outside and prior to the cell (this region is at a lower pressure than within the cell) exceeds those dissociations within because of the high-collision cross sections of the alkali halide cluster ions. In other words, the $n = 16$ population is depleted ($n = 16 \rightarrow n = 15$) prior to the cell. The most probable product ion ($n = 15$, see Figure 3) can then undergo collisional activation within the high-pressure region of the collision cell. Although bimolecular reactions occur outside the collision cell when a collision gas was

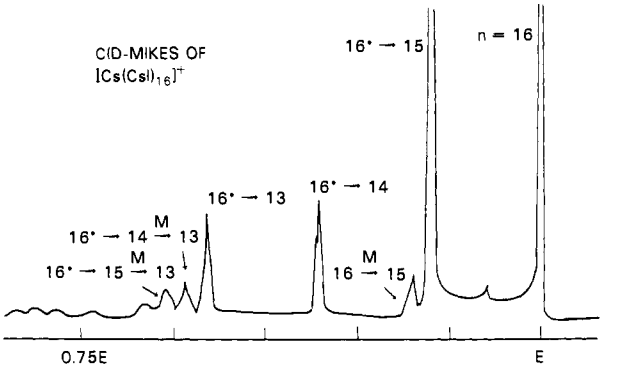

Figure 5. The CID-MIKES spectrum of $[Cs(CsI)_{16}]^+$ with a −1-kV collision-cell voltage applied. Two consecutive dissociations are identified.

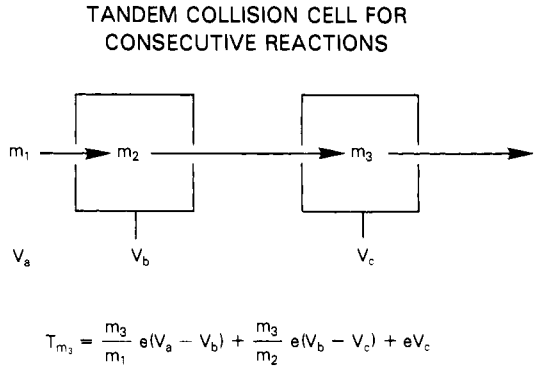

Figure 6. Tandem collision-cell arrangement and the ion kinetic energy of the second product ion when the first and the second collision cells have applied potentials of V_b and V_c, respectively.

used in this study, metastable ion notation will be used to differentiate those reactions occurring outside the cell.

In the absence of a collision-cell voltage (V_c), i.e., $V_c = 0$ the consecutive reactions (Figure 4, III and IV) $m_1^+ \rightarrow m_2^+ \rightarrow m_3^+$ cannot be distinguished from the reaction $m_1^+ \rightarrow m_3^+$ (netural products are not shown). With an applied cell voltage, the ion kinetic energy can be used to distinguish consecutive reactions occurring in two different second field-free regions (Figure 4, III and IV).

The MIKES spectrum shown in Figure 5 was obtained when the CsI $n = 16$ species was studied by CID-MIKES with −1.0 kV applied to the collision cell. Two consecutive reactions that have been identified involving the unstable intermediates, $n = 14$ and 15, are

$$[Cs(CsI)_{16}]^{+*} \rightarrow [Cs(CsI)_{15}]^+ + CsI$$

occuring prior to the cell followed by

$$[Cs(CsI)_{15}]^+ + M \rightarrow [Cs(CsI)_{13}]^+ + 2CsI$$

occurring within the cell, and similarly

$$[Cs(CsI)_{16}]^{+*} \rightarrow [Cs(CsI)_{14}]^+ + 2CsI$$

followed by

$$[Cs(CsI)_{14}]^+ + M \rightarrow [Cs(CsI)_{13}]^+ + CsI$$

The small peak between the precursor ion signal and the unimolecular component of $n = 16 \rightarrow 15$ is due to

$$[Cs(CsI)_{16}]^+ \rightarrow [Cs_2(CsI)_{15}]^+ + I$$

(D) Tandem Collision-Cell Spectroscopy. The observation of consecutive reactions within a single field-free region of the mass spectrometer suggests a novel instrumental concept for studying consecutive reactions. This concept uses two (or more) tandem collision cells in a field-free region following the first mass analyzer (or the second field-free region of a reverse-geometry mass spectrometer) to which voltages V_b and V_c may be applied as

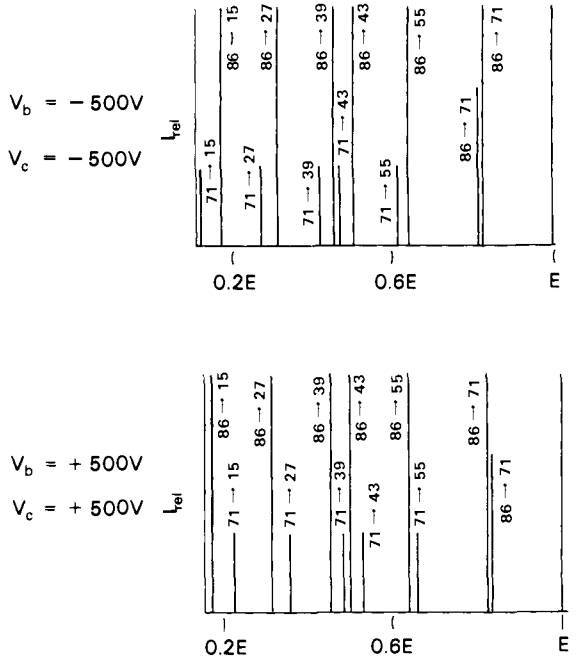

Figure 7. Simulated MIKES spectra of the consecutive reactions of $[C_5H_7O]^+$ (m/z 86) → $[C_5H_7O]^+$ (m/z 71) → fragments (m/z 55, 43, 39, 27, 15) with use of the tandem collision-cell arrangement depicted in Figure 6. The top simulated spectrum gives the average ion kinetic energies of the various fragment ions obtained with −500 V applied to both cells, and the bottom spectrum shows results obtained with +500 V applied to each cell.

shown in Figure 6. The average ion kinetic energy of the product ion from two consecutive dissociations within the tandem collision cells is

$$T_{m_3} = \frac{m_3}{m_1}e(V_a - V_b) + \frac{m_3}{m_2}e(V_b - V_c) + eV_c$$

where V_a is the acceleration voltage, m_1 is the atomic mass of the precursor ion, and m_2 and m_3 are the atomic masses of the first and second dissociation products. A recursion relation for the ith reaction product m_i in a system employing i tandem collision cells with corresponding applied voltages V_i is

$$T_{m_i} = \frac{m_i}{m_{i-1}}(T_{m_{i-1}} - V_ie) + V_ie$$

where T is the average kinetic energy of the subscripted reaction product.

We have simulated several MIKES spectra by using the tandem collision-cell concept from consecutive reactions previously studied on a triple-analyzer mass spectrometer.[21] The simulated MIKES spectra shown in Figure 7 could correspond to the CID of the m/z 86 molecular parent species ($C_5H_{10}O$) from 2-pentanone or 3-methyl-2-butanone followed by the consecutive CID of the m/z 71 species ($C_5H_7O^+$) to m/z 43 ($C_3H_7^+$), m/z 39 ($C_3H_3^+$), m/z 27 ($C_2H_3^+$), and m/z 15 (CH_3^+). The absolute ion abundances shown in Figure 7 have been chosen arbitrarily such that the metastable transition 86^{+*} → (daughter ion) outside of the cells is 100% abundant, collision-induced dissociation $86^+ + M \rightarrow 71^+$ within the first cell at potential V_b is 66% abundant, and the consecutive reaction product ions of the latter 71^+ product ion, $71^+ + M \rightarrow$ (daughter ion), are 33% abundant. These ion abundances distinguish the three reaction products. Figure 7 demonstrates the ion kinetic energy differences of the consecutive reaction product ions when the two tandem cell potentials are the same. A variety of potentials of varying magnitude and polarity could be used to deconvolute effectively the consecutive reaction product ions from interfering peaks that would normally be present in CID-MIKES spectra.

This low-resolution method for the study of consecutive reactions within the same field-free region of a reverse-geometry mass spectrometer may offer an economical advantage over triple-sector mass spectrometers and tandem mass spectrometers.[21] The method also is applicable to these more recent instrument geometries.

Concluding Remarks

The anomalous regions within the alkali halide secondary cluster ion mass spectra arise via the unicluster decay of conformationally unstable species to compact, low surface energy cluster ions. These data show that the structurally unstable $n = 14$ and $n = 15$ species preferentially decay to the compact $n = 13$ cubic-like structure. This unicluster decay accounts for the ion abundance enhancement at $n = 13$ and the low ion abundance of the $n = 14$ and 15 species that are observed in the conventional mass spectra from sector-type instruments where the cluster ion abundances are measured at times greater than 100 μs after ion emission. We assume this mechanism accounts for the other anomalous regions observed at higher n values.

Anomalous regions are absent in the TOF data[12,13] that show a continuous cluster ion abundance distribution. This latter smooth pseudexpoentially decaying distribution can be derived from a bond-breaking model[8,10] where the cluster ion abundance distribution is obtained by the statistical shattering of bonds in an infinite lattice by a primary particle.

These two time-resolved results (double-focusing and TOF mass spectrometry) lead to direct emission as one interpretation of the cluster ion emission mechanism for the alkali halide system. This mechanism instantaneously yields a smooth experimental[12,13] distribution (TOF data), which can be fit with a statistical bond-breaking model.[8,10] This emission step is followed (>200 ns) by the gas-phase unicluster decay of the unstable species that results in anomalous cluster ion abundance distributions reported in our work. This direct emission interpretation avoids the assumptions of recombination and lattice disintigration implicit in the alternative mechanism involving three steps. This latter sequence involves (a) the direct emission of small neutral clusters and cluster ions (monomers–trimers) that (b) recombine to form larger stable and unstable cluster ion species (centimers have been detected) giving a smooth distribution (TOF data) followed by (c) the unicluster decay of the unstable species to yield anomalous regions.

Recently, alkali halide cluster ion abundance distributions obtained by the nucleation of alkali halide vapor in cold He gas followed by cluster beam generation, electron ionization, and mass analysis have shown anomalous regions.[22] The enhanced cluster ion abundances corresponding to the cubic-like structures and stacked hexagonal rings are observed, as well as a lower abundance of the $n = 14$ and 15 species. The secondary cluster ion distributions show a greater $n = 14$ ion abundance than the $n = 15$ for NaI whereas the beam results show the opposite trend. In other words, the beam results show an enhancement at the $n = 15$ species of NaI due to the stacked hexagonal structure formed through nucleation that is not observed in the secondary ion studies. The data currently available from the time-resolved secondary ion studies[7,11-13] indicate that the direct emission of alkali halide cluster ions is the predominent secondary cluster ion emission mechanism,[10] although a recombination mechanism cannot be completely ignored especially with regard to other chemical systems.[23]

Registry No. NaI, 7681-82-5; CsI, 7789-17-5.

(21) D. J. Burinsky, R. G. Cooks, E. K. Chess, M. L. Gross, *Anal. Chem.*, **54**, 295-299 (1982).

(22) K. Sattler, "Proceedings of the 13th International Symposium on Rarefield Gas Dynamics", Novosibirsk, USSR, 1982; K. Sattler, J. Muhlback, P. Pfau, R. Pflaum, E. Recknagel, and T. P. Martin, unpublished work.

(23) B. J. Garrison and N. Winograd, *Chem. Phys. Lett.*, 97, 381-386 (1983).